EAST EUROPEAN JOURNAL OF PHYSICS. **2.** 267-275 (2025)
DOI:10.26565/2312-4334-2025-2-32 ISSN 2312-4334

ANALYSIS OF AC RESPONSE AND CHARGE TRANSPORT MECHANISMS IN DOUBLE-LAYER AND TRIPLE-LAYER SOLAR CELL ARCHITECTURES

Hmoud Al Dmour
Department of Physics, Faculty of Science, Mu'tah University, Mu'tah 6170, Jordan
Corresponding Author e-mail: hmoud79@mutah.edu.jo
Received February 28, 2025 revised April 18, 2025; accepted April 28, 2025

This work investigates the effect of the ruthenium dye (Ru -dye) layer on electrical properties of solar cells based on the nc-TiO_2 semiconducting polymer heterojunction. In TLSCs (P3HT/Ru-dye/nc-TiO_2 solar cells), when the measurement frequency is decreased from 10 Hz to 0.1 Hz, a three-orders-of-magnitude increase in capacitance is observed. It is attributed to the dominance of diffusion capacitance the measurements, which indicates enhanced charge carrier dynamics and contribute to better performance and improved efficiency. In contrast, in the same frequency range, DLSCs (P3HT/nc-TiO_2 solar cells) exhibits a one-order-of-magnitude increase in capacitance, ascribed to the dominance of depletion capacitance. Thus, DLSCs likely suffer from low carrier injection, high recombination losses, and ultimately lower efficiency. The Cole-Cole curves are plotted for applied voltages ranging from 0 to 1.5 V and frequencies from 20 Hz to 1 MHz. At zero bias, while there is evidence of a relaxation process in TLSCs, this is not as clear for DLSCs. This is related to the effect of the Ru-dye inserted between the P3HT and nc-TiO_2 layers (TLSC), which facilitates better charge carrier generation and transport.
Keywords: *Solar Cells; Diffusion capacitance; Charge carreris; Efficiency; Interfaces*
PACS: 84.60.Jt ,73.40.kp , 84.37.q.42.60.Lh. 72.20.Jv

1. INTRODUCTION

The performance of solar cells based on electron and hole transport materials is influenced by many factors [1-3]. One of the main factors is the quality of the interfacial layer formed between the components of solar cells. This interface plays a very important role in solar cells. In the case of inorganic solar cell semiconductors, extensive studies on this interface have provided valuable knowledge, leading the electronics industry to improve fabrication techniques and develop better-performing, longer-lasting integrated circuits [3]. For inorganic/organic solar cells, the interface is especially important as well, since it is commonly found that in organic devices, the same semiconductor behaves very differently depending on the dielectric material used and the interface thus formed, such as TiO_2 and P3HT [4,5]. Therefore, various organic and inorganic interface modifiers have been used to enhance the efficiency of hybrid TiO_2/P3HT solar cells in order to improve charge separation and molecular arrangement. Some of these modifiers include optimized fabrication, dopants, and tailored interfacial interactions, which further enhance charge transport and light absorption, advancing organic photovoltaics [6,7]. The interface between these components of solar cells influences solar cell efficiency, stability, and resilience in harsh weather conditions, such as heavy rain or snowstorms.

In this study, we present an investigation into the frequency and voltage dependence of the admittance in solar cells based on the nc-TiO_2 semiconducting polymer heterojunction. Section II outlines the theoretical framework of the conductance technique applied to solar cells. Section III details the experimental procedures for device fabrication and characterization. In Section IV, we analyze and discuss the experimental results in relation to the theoretical concepts introduced earlier. Our data analysis highlights the role of interface states and the impact of dye layers on device performance.

2. THEORTCAL SECTION

To understand the behavior of a heterojunction solar cell it is useful to consider the behavior of polar dielectric in an alternating electric field using these references (8-11). If a small sinusoidal voltage of angular frequency ω is applied to a parallel plate capacitor filled with such a material, then the capacitance, C, is given by

$$C = \frac{\varepsilon_r \varepsilon_o A}{d} \tag{1}$$

where ε_r is the relative permittivity of the dielectric, ε_o the permittivity of free space, A the place area and d the plate separation.

When measured over a wide range of frequencies from 10^2 to 10^{10} Hz, ε_r shows a strong frequency dependence, see Figure 1.

At low frequencies ε_r is essentially constant and equal to ε_s the static or low-frequency dielectric constant. As the frequency increase and permanent dipoles in the dielectric cease to be able to follow the voltage, then dispersion occurs

Cite as: H. Al Dmour, East Eur. J. Phys. 2, 267 (2025), https://doi.org/10.26565/2312-4334-2025-2-32

and ε_r decrease to ε_∞, the high frequency dielectric constant, which reflects induced polarization corresponding to atomic and electron displacements in the alternating electric field. Also shown dotted at low frequency is a possible contribution from interfacial polarization. In our solar cells, this is an important contribution for interfaces formed between the components of devices.

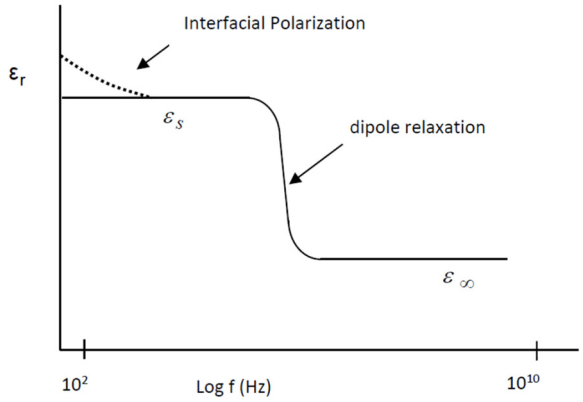

Figure 1. Frequency dependence of ε_r for a polar dielectric. The dotted curve shows the effect of interfacial polarization

- **Interfacial polarization (Maxwell –Wagner Effect)**

In a homogenous dielectric with conductivity σ and permittivity ε, the current density of the system is determined using Maxwell's equation

$$J = \sigma E + \varepsilon \frac{dE}{dt} \tag{2}$$

where E is the electric field. For an alternating applied voltage $V=V_O e^{j\omega t}$ and since $E=\frac{V}{d}$, equation (2) may be written as

$$J = j\omega \left(\varepsilon - j\frac{\sigma}{\omega}\right)\frac{V}{d}. \tag{3}$$

Hence the capacitor may be represented by a complex capacitance per unit area, C^*, where

$$C^* = \frac{\varepsilon - j\frac{\sigma}{\omega}}{d} \tag{4}$$

.

If the capacitor consists of two different materials, they may be characterized by their thickness (d_1,d_2), conductivity (σ_1, σ_2) and permittivity ($\varepsilon_1, \varepsilon_2$) (Figure 2).

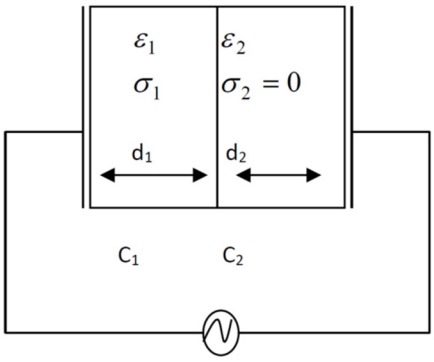

Figure 2. An inhomogenous capacitor formed from two different dielectrics

The two materials will have capacitances C_1 and C_2 in series and if $\sigma_2 = 0$, then

$$C_1 = \frac{\varepsilon_1 - j\frac{\sigma}{\omega}}{d} \tag{5}$$

and

$$C_{2=}\frac{\varepsilon_2}{d_2} \tag{6}$$

so that the total capacitance C_T is given by

$$C_T^* = \frac{C_1 C_2}{C_1 + C_2} = \frac{\varepsilon_T^*}{d_1 + d_2} \tag{7}$$

where ε_T^* is the apparent complex permittivity.

The apparent permittivity ε_T^* is given by

$$\varepsilon_T^* = \frac{(\varepsilon_1 - j\frac{\sigma}{\omega})\varepsilon_2}{(\varepsilon_1 - j\frac{\sigma}{\omega})f_2 + \varepsilon_2 f_1} \tag{8}$$

where $f_1 = \frac{d_1}{d_1 + d_2}$ and $f_2 = \frac{d_2}{d_1 + d_2}$

When $\omega \to 0$, $\varepsilon_T^* \to \varepsilon_s$, the apparent value of the static permittivity

$$\varepsilon_S = \frac{\varepsilon_2}{f_2}. \tag{9}$$

When $\omega \to \infty$, $\varepsilon_T^* \to \varepsilon_\infty$, the apparent value of the high frequency permittivity

$$\varepsilon_\infty = \frac{\varepsilon_2 \varepsilon_1}{\varepsilon_1 f_2 + \varepsilon_2 f_1}. \tag{10}$$

By substitution it can be shown that

$$\frac{\varepsilon_T^* - \varepsilon_\infty}{\varepsilon_S - \varepsilon_\infty} = \frac{-j\frac{\sigma}{\omega}}{\varepsilon_1 f_2 + \varepsilon_2 f_1 - j\frac{\sigma}{\omega} f_2} \tag{11}$$

or

$$\frac{\varepsilon_T^* - \varepsilon_\infty}{\varepsilon_S - \varepsilon_\infty} = \frac{1}{1 + j\omega\tau} \tag{12}$$

where $\tau = \frac{\varepsilon_1 f_2 + \varepsilon_2 f_1}{\sigma f_2}$. Here τ is the relaxation time of the double-layer capacitor structure. Rearranging equation (12) then yields

$$\varepsilon_T^* = \varepsilon_\infty + \frac{\varepsilon_S - \varepsilon_\infty}{1 + j\omega\tau} \tag{13}$$

or

$$\varepsilon_T^* = \varepsilon_\infty + \frac{\varepsilon_S - \varepsilon_\infty}{1 + \omega^2\tau^2} - \frac{j\omega\tau(\varepsilon_s - \varepsilon_\infty)}{1 + \omega^2\tau^2}. \tag{14}$$

Equation (14) may be simplified to

$$\varepsilon_T^* = \varepsilon' - j\varepsilon'' \tag{15}$$

where the real part

$$\varepsilon' = \varepsilon_\infty + \frac{\varepsilon_S - \varepsilon_\infty}{1 + \omega^2\tau^2} \tag{16}$$

And the imaginary part

$$\varepsilon'' = \frac{\omega\tau(\varepsilon_s - \varepsilon_\infty)}{1 + \omega^2\tau^2}. \tag{17}$$

These represent exactly the format of the Debye equation for a single relaxation time process and show that ε' and ε'' are frequency dependent (Figure 3).

The Debye equation can be rearranged to eliminate ω, yielding

$$(\varepsilon'(\omega) - \frac{\varepsilon_s + \varepsilon_\infty}{2})^2 + (\varepsilon''(\omega))^2 = \frac{1}{4}(\varepsilon'' - \varepsilon_\infty)^2. \tag{18}$$

This is an equation for a circle when $\varepsilon''(\omega)$ is plotted against $\varepsilon'(\omega)$. Such a plot (Figure 4) is known as a Cole-Cole plot.

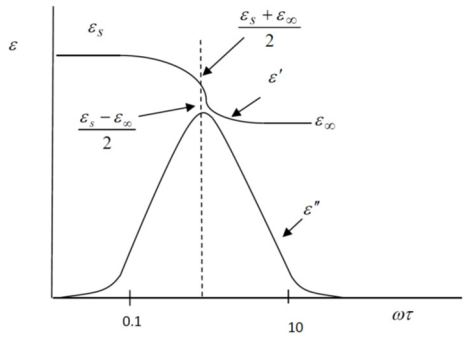

Figure 3. Relaxation spectrum of the inhomogeneous capacitor

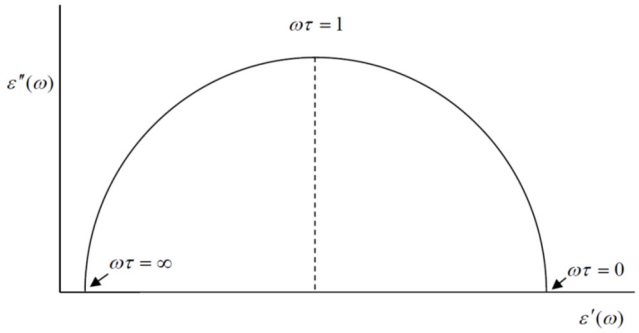

Figure 4. A Cole-Cole plot of $\varepsilon''(\omega)$ versus $\varepsilon'(\omega)$ of a single relaxation time process

If there are two semicircles in the Cole –Cole plot, then this provides evidence of two process occurring in the device (Figure 5).

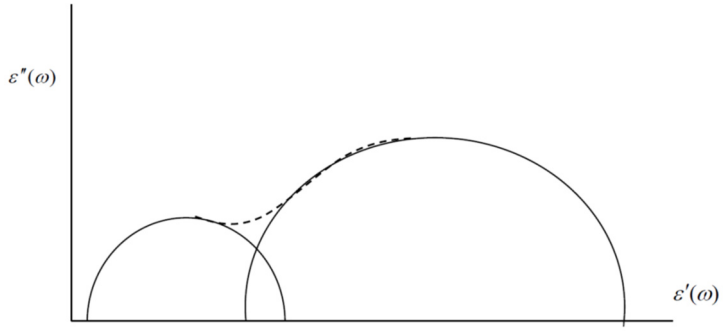

Figure 5. Cole-Cole plot of $\varepsilon''(\omega)$ versus $\varepsilon'(\omega)$ with two processes occurring in the device

In an interpenetrating system such as a bulk heterojunction solar cell, then the simple two-layer model breaks down and the device is likely to be characterized by a distribution of relaxation times. By analogy with polar dielectrics with a distribution of relation times we may now write the complex permittivity ε_T^* as

$$\varepsilon_T^* = \varepsilon_\infty + \frac{\varepsilon_S - \varepsilon_\infty}{1 + j\omega\tau^{(1-\alpha)}} \tag{19}$$

where α is a parameter describing the distribution. When α =0 the single relaxation time response is recovered. When 0< α <1, the effect of the distribution of relaxation times is to broaden and flatten the Cole-Cole plot as shown in Figure 6.

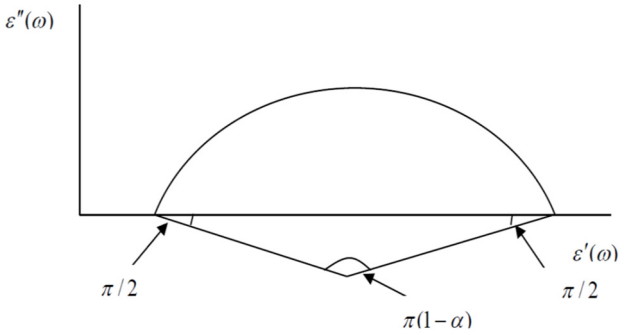

Figure 6. The effect of the distribution of relaxation time on the Cole-Cole plot

3. EXPERIMENTAL METHOD

Figure 7 shows the molecular structure of the materials used in our solar cells. The devices were made using fluorine-doped tin oxide (SnO_2:F) electrodes with a compact TiO_2 layer added by spray pyrolysis according to [7]. A nanocrystalline π / 2 TiO_2 (nc-TiO_2) paste acted as the active layer, sensitized with ruthenium dye ($RuL_2(NCS)_2$:2 TBA) from Solaronix Co., Switzerland. The p-type semiconductor, P3HT, was from Sigma-Aldrich Ltd. Similar devices without the ruthenium dye were also fabricated for comparison. To fabricate the cells, the SnO_2:F/TiO_2 substrates were cleaned

thoroughly with Decon 90 soap, rinsed with tap, hot, and ultrapure water, and dried. The nc-TiO_2 paste was spread on the surface, dried in air, and heated to 450°C for 30 minutes to form a porous anatase layer about 2 µm thick. This layer was soaked in a ruthenium dye solution for 48 hours, then rinsed with ethanol and dried under nitrogen. The P3HT layer was applied on top by spin-coating a chloroform solution of P3HT at 1000 rpm. A gold layer (~50 nm thick) was deposited as the top electrode with a device area of 3 mm². Electrical testing was done using a Solartron 1260 Frequency analyzer. Capacitance and conductance were measured across frequencies from 100 Hz to 1 MHz at room temperature. Capacitance-voltage measurements were taken in the range of +2.5 V to −2.5 V at 0.1 V steps and a fixed frequency of 100 Hz. Voltage bias was applied to the SnO_2:F electrode, with forward bias from 0 V to −2.5 V and reverse bias from +2.5 V to 0 V.

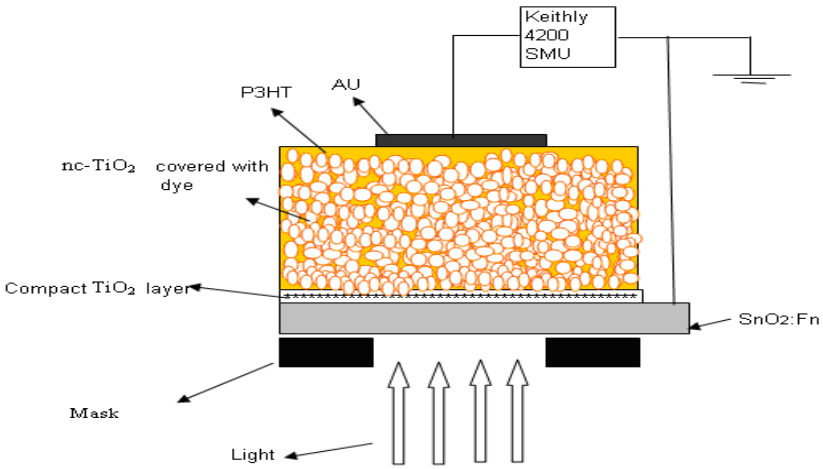

Figure 7. Schematic representation of the solar cell structure tested under illumination

4. RESULTS AND DISCUSSION

Figure 8 shows the difference in DC characteristics of TLSCs and DLSCs in both dark and illuminated conditions. In the dark, TLSCs have a strong rectification ratio of about 3000 at +1V, with a low reverse current, while DLSCs show a much lower rectification ratio of 10 at -0.8V.

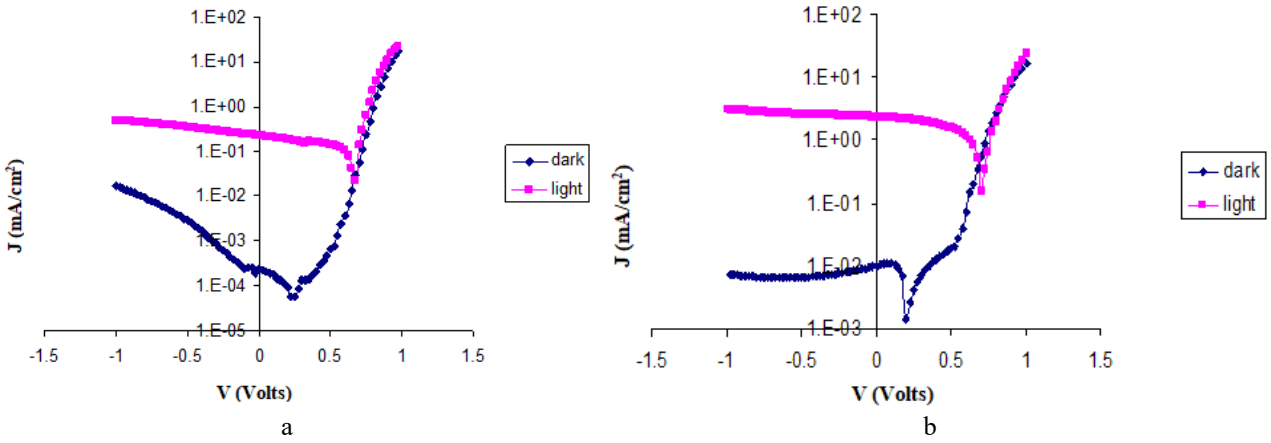

Figure 8. J –V characteristics of (a) DLSC and (b) TLSC device under illumination and dark conditions

Both types of devices turn on at around 0.65V, but TLSCs start conducting strongly at 0.65V, whereas DLSCs reach a high current (~10mA/cm²) at 0.8V. Under illumination with a halogen lamp, TLSCs produce a higher open-circuit voltage (Voc) of 0.73V, a much greater short-circuit current density (Jsc) of 2.3mA/cm², a fill factor (FF) of 49%, and a power conversion efficiency (PCE) of 1.1%. In contrast, DLSCs achieve a Voc of 0.68V, a significantly lower Jsc of 0.22mA/cm², an FF of 46%, and a PCE of just 0.09%. The higher Jsc in TLSCs suggests better charge collection efficiency. The DLSCs show some variation in Voc (0.65V–0.68V), likely due to an electric field at the nc-TiO_2/P3HT interface, as previously reported for similar cells. Both device types show increased current under illumination at high forward bias, indicating photoconductivity. Overall, TLSCs outperform DLSCs in Voc, Jsc, and PCE, making them a stronger choice for solar cell applications.

The capacitance versus frequency characteristics of DLSCs as a function of the applied voltage were presented in Figure 9. At high frequency (0.1MHz), the capacitance was ~188 pF and almost constant as the applied voltage increased. At low frequency, the loss appears to become almost constant capacitance was over 3 orders of magnitude greater and dependent on the voltage applied to the device. For an applied voltage of 0V, the capacitance measured at 1Hz was 156nF

and increased to 448 nF at -0.4V therefore remaining constant for further increases in forward bias. Figure 9-b shows the loss-frequency relationship for a DLSC with different voltages applied to the SnO_2:F electrode. With -0.8V applied, the loss at 0.1MHz was ~290pF, but increasing, following a law of the form $\omega^{-0.83}$, to ~1300nF at 1Hz. Similar behavior was observed for ~ 0.4V and 0V.

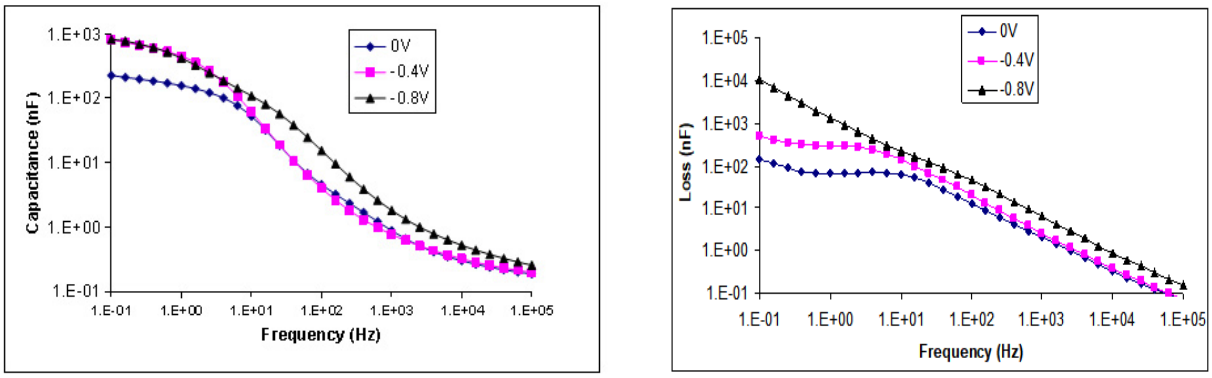

a b

Figure 9. a) Logarithmic plot of capacitance and b) loss versus frequency characteristics of DLSC under different voltages applied to the SnO_2:F electrode

In Figures 10, the results presented in Figure 9 are replotted as Cole-Cole plot. Figure 10 shows the Cole-Cole plot of DLSC. In this figure, the curves show clear dispersion between about 1Hz and 100 Hz, corresponding to the region of almost constant loss in figure 9. At low frequency, a second process is observed which suggest additional dispersion although the almost constant capacitance in this region suggests that it arises from a DC loss in the device. This view is reinforced in Figure 10-b and 10-c where application of a forward voltage increases this component significantly. At the highest frequencies (100Hz TO 10kHz), there is a tendency for the plots to converge at a capacitance of 188pF, which corresponds to the device thickness.

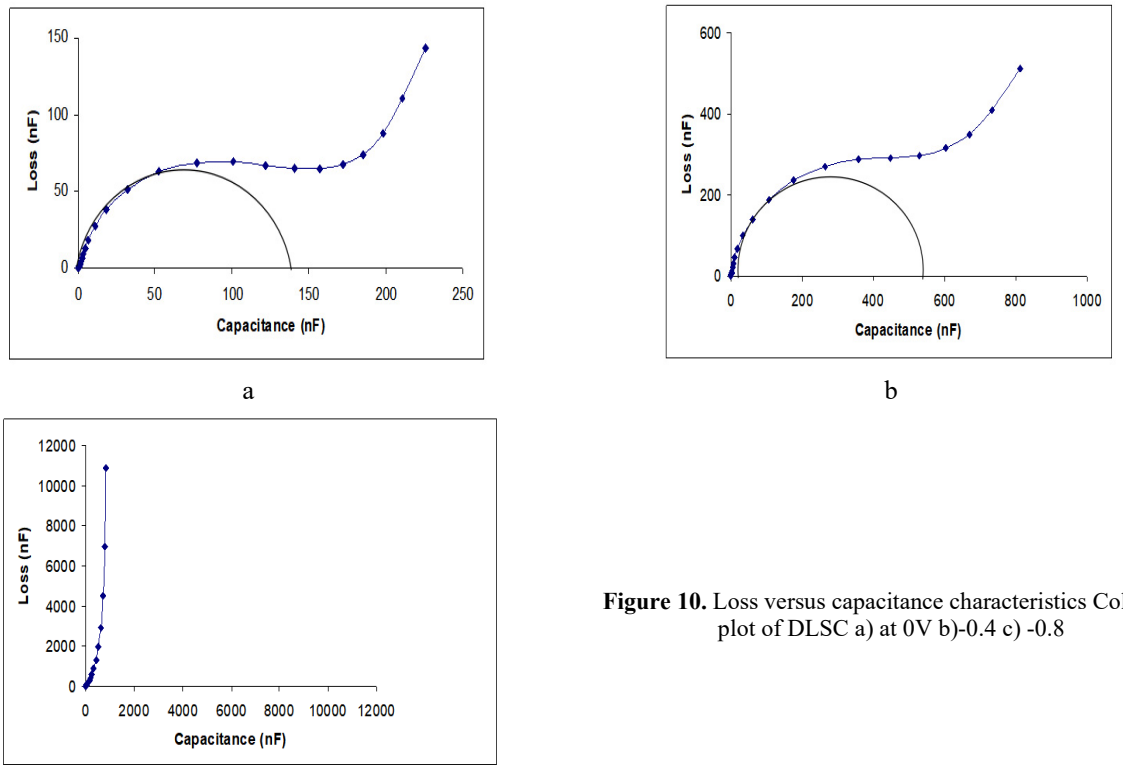

a b

c

Figure 10. Loss versus capacitance characteristics Cole-Cle plot of DLSC a) at 0V b)-0.4 c) -0.8

The capacitance-voltage (C-V) characteristics of DLSCs were also measured at two different frequencies, namely 10 KHz and 1 Hz. The results are shown in Figures 11-a and 11-b respectively. As can be seen, capacitance was virtually independent of the applied voltage when the device was under reverse bias, but increased rapidly at -0.6V at high frequency and at -0.2V for the lower frequency. In both cases, this capacitance passes through a maximum and decreases rapidly for further increase in forward bias.

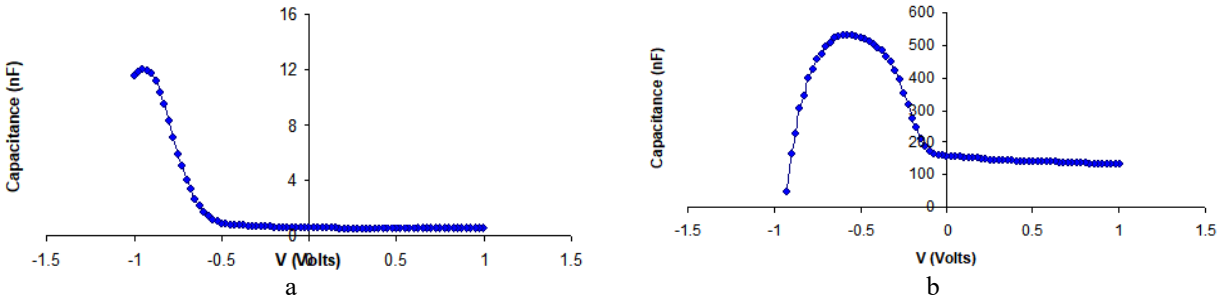

a b

Figure 11. Capacitance-voltage characteristics of DLSC at (a) 10KHz and (b) 1Hz

Figure 12 shows capacitance versus frequency characterization of a TLSC as a function of the voltage applied to the SnO_2:F electrode. For an applied voltage of 0V, the high frequency capacitance was ~189 pF for a frequency of 0.1 MHz which is similar to the high frequency capacitance of a DLSC. However, comparing Figure 9 and Figure 12-a, the high frequency capacitance of the TLSC was more strongly dependent on the applied voltage, especially at frequencies below 0.1 MHz. However, there was an increase in the low frequency capacitance compared to DLSCs as follows:

1. For an applied voltage of 0V, the capacitance of DLSC at 1Hz was ~157 nF in contrast to 42nF for TLSC.
2. For an applied voltage of -0.8V, the low frequency capacitance of TLSCs at 1Hz was ~3340nF and hence significantly greater than ~471 nF for DLSCs.

Figure 12-b shows the loss–frequency characteristics of the TLSCs with different bias voltages applied to the SnO_2:F electrode. At 0.1 MHz, the loss showed stronger voltage dependence in the TLSC compared with the DLSC. At 1Hz, this dependence was much more marked. The loss in the TLSCs increased by more than 3 orders of magnitude to ~ 2.2×10^4 nF for an applied voltage of -0.8V.

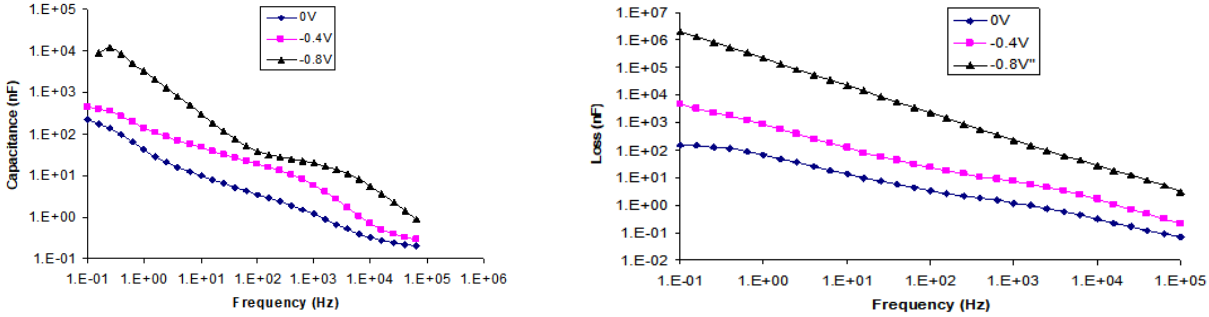

a b

Figure 12. a) Logarithmic plot of (a) capacitance and b) loss versus frequency characteristics of TLSC versus frequency characteristics under different voltages applied to the SnO_2:F electrod*e*

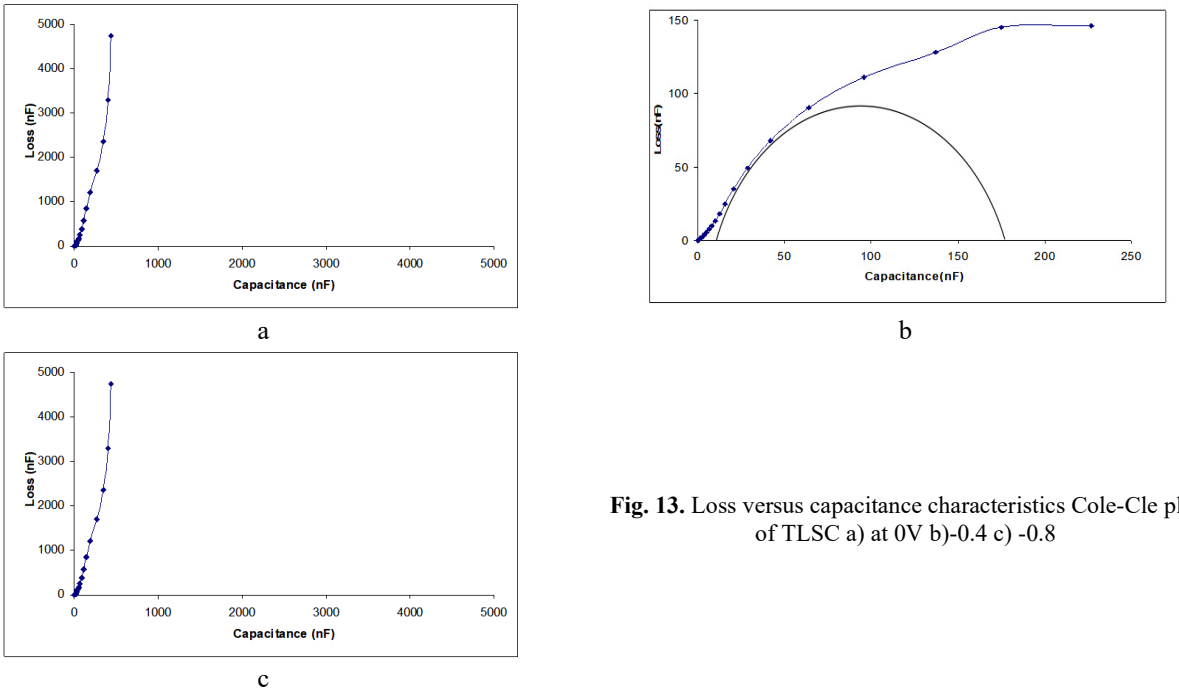

a b

c

Fig. 13. Loss versus capacitance characteristics Cole-Cle plot of TLSC a) at 0V b)-0.4 c) -0.8

Figures 13 show the Cole-Cole plots for the TLSCs with a different applied voltage. At zero bias, while there is evidence for a relaxation process, this is not so clear as for the DLSC. Here the DC loss is already beginning to dominate the dispersion and clearly does so when the voltage applied was increased from 0V to -0.4V and -0.8V.Figure 14 shows the C-V characteristic of a TLSC at at two different frequencies, namely 10 KHz and 1 Hz. The capacitance was independent of the applied voltage when the device was in reverse bias, but increased rapidly to a maximum value in forward bias as seen in the DLSCs (figure 11). Interestingly in the TLSC, the maximum capacitance reached was lower than in DLSCs (~4 nF compared to 13 nF) and occurred at a lower voltage -0.85V. On other hand , Figure 14 shows capacitance-voltage measurements on a TLSC at 1Hz . The result behave a steadily increasing capacitance for increasing forward bias, reaching 1600nF at 0.5V and much higher, therefore, than observed in DLSC under corresponding conditions.

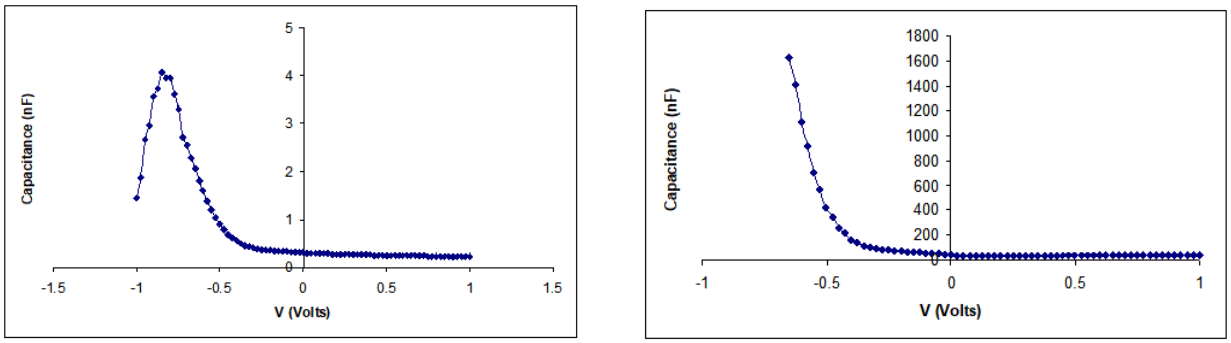

a b

Figure 14. Capacitance-voltage characteristics of TLSC at (a) 10KHz and (b) 1Hz

5. DISCUSSION

The J-V characteristics (Figure 8) clearly show that TLSCs show better performance in comparison with DLSCs. Under illumination, TLSCs produce a Voc of 0.73V, a Jsc of 2.3 mA/cm², and a PCE of 1.1%, while DLSCs produce a Voc of 0.68V, a Jsc of 0.22 mA/cm², and a PCE of just 0.09%. The higher efficiency in TLSCs is attributed to the presence of the Ru-dye layer, which acts as a sensitizer and facilitates better charge carrier generation and transport. That is accompanied by higher Jsc and Voc in TLSCs, indicating improved charge collection efficiency and reduced recombination losses at the interface [11-14]. In contrast, DLSCs suffer from poor charge separation and high recombination, leading to lower efficiency.

The AC results, including capacitance-frequency (C-f) measurements, loss-frequency characteristics, and Cole-Cole plots, provide further insights into the charge transport mechanisms and the role of the Ru-dye layer. At high frequencies (0.1 MHz), the capacitance is nearly constant (~188 pF for DLSCs and ~189 pF for TLSCs) and represents the geometric capacitance of the device, dominated by the bulk regions of P3HT and nc-TiO_2. However, at low frequencies (1 Hz), the capacitance behavior diverges significantly between DLSCs and TLSCs. In DLSCs, the capacitance increases with applied voltage, reflecting the dominance of depletion capacitance, which is associated with charge accumulation and recombination at the P3HT/nc-TiO_2 interface. This behavior is consistent with the poor charge separation and high recombination losses observed in the DC results. In contrast, TLSCs exhibit a much larger increase in capacitance at low frequencies, which is attributed to diffusion capacitance, indicating efficient charge carrier dynamics and reduced recombination. This is consistent with the improved charge collection efficiency and higher Jsc observed in the DC results. The capacitance-voltage (C-V) characteristics at different frequencies further support these findings. At 10 kHz, the capacitance in TLSCs reaches a maximum of ~4 nF at -0.85V, which is lower than the maximum capacitance observed in DLSCs (~13 nF). This indicates better charge control in TLSCs, consistent with the improved charge transport and reduced recombination observed in the DC results. At 1 Hz, the capacitance in TLSCs increases steadily with forward bias, reaching 1600 nF at 0.5V, which is significantly higher than in DLSCs. This reflects the dominance of diffusion capacitance in TLSCs due to improved charge carrier dynamics.

6. CONCLUSIONS

The DC and AC results are closely interrelated and provide complementary insights into the performance and charge transport mechanisms of the solar cells. The DC results demonstrate that TLSCs have better steady-state performance, with higher Voc, Jsc, and PCE, while the AC results reveal that this improvement is due to better charge separation, reduced recombination, and more efficient charge transport facilitated by the Ru-dye layer. The Ru-dye acts as a sensitizer, enhancing charge injection into nc-TiO_2 and reducing recombination losses, which leads to superior charge carrier dynamics and overall device efficiency. The combination of DC and AC analysis provides a comprehensive understanding of the charge transport mechanisms and highlights the critical role of the Ru-dye layer in improving the performance of TLSCs. This integrated approach underscores the importance of interfacial modifications, such as the incorporation of a Ru-dye layer, in optimizing the performance of organic-inorganic hybrid solar cells.

ORCID

Hmoud Al Dmour, https://orcid.org/0000-0001-5680-5703

7. REFERENCES

[1] L. Bhattacharya, and M. Caspary, "Factors influencing charge transport at perovskite–charge transport layer interfaces: current strategies, challenges, and perspectives based on first-principles studies," J. Phys. D: Appl. Phys; **57**, 412001 (2024). https://doi.org/10.1088/1361-6463/ad4dae

[2] H. Al-Dmour, and D.M Taylor, "Effect of properties of NC-TiO_2 grains on the performance of organic/inorganic solar cells," JOR, **19**, 587-596 (2023). https://doi.org/10.15251/JOR.2023.195.587

[3] N. Dey, M. Reza, A. Ghosh, H, Al-Dmour, *et al.*, "Optimization of Sr3NCl3-based perovskite solar cell performance through the comparison of different electron and hole transport layers," J. Phys. Chem. Solids, **196**, 112386 (2025) https://doi.org/10.1016/j.jpcs.2024.112386

[4] N. Juneja, *et al.*, "Sb_2S_3 solar cells with a cost-effective and dopant-free fluorene-based enamine as a hole transport material," Sustain Energ Fuels, **6**, 3220 (2022). https://doi.org/10.1039/d2se00356b

[5] H. Al Dmour, and D. Taylor, "Small-signal response of nanocrystalline-titanium dioxide/poly(3-hexylthiophene) heterojunction solar cells," Thin solid Film, **519**(22), 8135-8138 (2011). https://doi.org/10.1016/j.tsf2011.06.009

[6] Z. Wang, C. Gong, C. Zhang, C. Zhao, T.-S. Su, H. Li, and H. Zhang, "Recent Advances in Interfacial Engineering for High-Efficiency Perovskite Photovoltaics," DeCarbon, 1-47 (2025) https://doi.org/10.1016/j.decarb.2025.100107

[7] N. Saleh, S. Al-Trawneh, H. Al-Dmour, *et al*., "Effect of Molecular-Level Insulation on the Performance of a Dye-Sensitized Solar Cell: Fluorescence Studies in Solid State," J. Fluoresc. **25**, 59–68 (2015). https://doi.org/10.1007/s10895-014-1479-8

[8] S.M. Sze, *Physics of Semiconductor Devices*, 2nd edition, (Wiley-Interscience, 1981).

[9] E.H. Nicollian, and J.R. Brews, *MOS (Metal Oxide Semiconductor) Physics and Technology*, (Wiley Interscience, Wiley Classics Library edition, 1981)

[10] M. Madanat, A. Al-Tabbakh, M. Alsa'eed, H. Al-Dmour, and M. Mousa, "Application of Murphy – Good Plot Parameters Extraction Method on Electron Emission from Carbon Fibers," Ultramicroscopy, **234**, 113479 (2022). https://doi.org/10.1016/j.ultramic.2022.113479

[11] H. Zhou, M. Aftabuzzaman, M. Masud, S. Kang, and H.K. Key, "Materials and Fabrication Strategies for High-Performance Dye-Sensitized Solar Cells: Comprehensive Comparison and Perspective," ACS Energy Letters, **10**(2), 881-895 (2025). http://dx.doi.org/10.1021/acsenergylett.4c03579

[12] N. Lal Dey, M. Reza, Av. Ghosh, H. Al-Dmour, *et al*., "Optimization of Sr3NCl3-based perovskite solar cell performance through the comparison of different electron and hole transport layers," J, Fluoresc, **25**, 59–68 (2015). https://doi.org/10.1007/s10895-014-1479-8

[13] N.L. Dey, Md.S. Reza, A. Ghosh, H. Al-Dmour, M. Moumita, Md.S. Reza, S. Sultana, *et al*., "Optimization of Sr_3NCl_3-based perovskite solar cell performance through the comparison of different electron and hole transport layers," J. Phys. Chem. Solids, **96**, 112386 (2025). https://doi.org/10.1016/j.jpcs.2024.112386

[14] H. Al Dmour, "Capacitance response of solar cells based on amorphous Titanium dioxide (A-TiO2) semiconducting heterojunctions,"AIMS Mater. Sci, **8(2)**, 261-270 (2021). https://doi.org/0.3934/matersci.2021017

АНАЛІЗ ВІДГУКУ ЗМІННОГО СТРУМУ І МЕХАНІЗМІВ ПЕРЕНОСУ ЗАРЯДУ В ДВОШАРОВИХ І ТРИШАРОВИХ АРХІТЕКТУРАХ СОНЯЧНИХ ЕЛЕМЕНТІВ

Хмуд Аль Дмур

Кафедра фізики, факультет природничих наук, Університет Мута, Мута 6170, Йорданія

У цій роботі досліджується вплив шару рутенієвого барвника (Ru-барвник) на електричні властивості сонячних елементів на основі напівпровідникового полімерного гетеропереходу nc-TiO_2. У TLSC (сонячні елементи P3HT/Ru-барвник/nc-TiO_2) при зменшенні частоти вимірювань з 10 Гц до 0,1 Гц спостерігається збільшення ємності на три порядки. Це пояснюється домінуванням дифузійної ємності у вимірюваннях, що вказує на покращену динаміку носіїв заряду та сприяє кращій продуктивності та підвищенню ефективності. На противагу цьому, в тому ж діапазоні частот, DLSC (сонячні елементи P3HT/nc-TiO_2) демонструють збільшення ємності на один порядок, що пояснюється домінуванням виснажливої ємності. Таким чином, DLSC, ймовірно, страждають від низької інжекції носіїв заряду, високих втрат на рекомбінацію та, зрештою, нижчої ефективності. Криві Коула-Коула побудовані для прикладених напруг в діапазоні від 0 до 1,5 В та частот від 20 Гц до 1 МГц. При нульовому зміщенні, хоча є ознаки процесу релаксації в TLSC, це не так очевидно для DLSC. Це пов'язано з ефектом Ru-барвника, вставленого між шарами P3HT та nc-TiO_2 (TLSC), що сприяє кращому генеруванню та транспорту носіїв заряду.

Ключові слова: *сонячні елементи; дифузійна ємність; носії заряду; ефективність; інтерфейси*